Supersymmetric jets from toponium decay

Dan Haim
Physics Department, University of Illinois at Urbana-Champaign, 1110 West Green Street, Urbana, Illinois 61801
(Received 16 November 1987; revised manuscript received 10 March 1988)

A Monte Carlo simulation for the supersymmetric (SUSY) processes $e^+e^- \to \Theta \to g\tilde{g}\bar{\gamma}$ and $g\tilde{g}\bar{\gamma}$, where Θ is a $t\bar{t}$ bound state, has been carried out to a fully hadronized final state. In the search for a unique signature, a detailed comparison to the non-SUSY processes $e^+e^- \to \Theta \to ggg$ and $gg\gamma$ was performed, in both jet analysis and the shape of the events. We found that in the SUSY modes the missing energy is very large compared to the non-SUSY ones. The jet spectrum of the two modes is quite different and is related to the jet's origin. The SUSY modes have many more four- and five-jet events. The number of B mesons and neutrinos is also enhanced in the SUSY mode. The study included dependence on the masses of the top quark and the $\tilde{g}$. A method to determine the $\tilde{g}$'s mass, using the missing-energy distribution, has been developed.

I. INTRODUCTION

In the past few years a great deal of effort has been made to look for "new physics" at high-energy colliders. Along with that search, the search for the top quark intensified. In this paper we incorporate the above two topics, and investigate the processes[1,2] $e^+e^- \to \Theta \to g\tilde{g}\tilde{k}$ (Fig. 1), where Θ is a $t\bar{t}$ bound state and $\tilde{k}$ can be either a gluino or a photino. The hope is to be able to predict a unique signature for the supersymmetric decay of the $^3S_1$ bound state of $t\bar{t}$. The discussion is based on the assumption that the top quark will be seen before supersymmetry (SUSY) is discovered.

The model that is used in this study is the simplest $N=1$ supersymmetry. We assume that both the left- and right-handed scalar quarks are mass degenerate and that the photino is the lightest SUSY particle with a mass[3] of 5 GeV. The matrix element for the Θ decay was calculated using the computer program REDUCE, without restrictions on the masses. The result fully agrees with Keung's[2] result in the limit of a massless photino.

The paper starts by reviewing the Monte Carlo program that was used to generate 1000 hadronized events of each type. The hadronization method is described in detail in Refs. 4 and 5. We then analyze the results and compare them to the non-SUSY processes $e^+e^- \to \Theta \to ggk$, where k is either a gluon or a photon. The comparison is made in the jet analysis and the shape of the events. A special role is taken by the missing energy, which appears to be the most important parameter in distinguishing SUSY. The jets were also investigated in relation to the original parton from which they were created. In the final stage of the hadronization, we allowed the decay of heavy mesons into light mesons. Among the final-state particles we find π, η, and K mesons, together with the e and the μ leptons, the stable baryons, and the photons.

The B hadrons are an important and interesting component of the final state. Because not all B-containing hadrons have yet been discovered experimentally, an artificial spectrum of masses was created using theoretical models. The B-meson masses of Godfrey and Isgur[6] were used, and the B-baryon masses were calculated according to the formula of De Rújula, Georgi, and Glashow[7] (see details in Ref. 5). We kept the B hadrons undecayed since there is not a good model yet, for their partial decay modes, and we can also learn about their numbers in the final state. We expect that most of the B's will come from the $\tilde{g}$ decay, and not from the gluon. The reason for this is the high probability that a hard gluon will split into two gluons, early in the cascade, rather than to quark-antiquark pair. The $\tilde{g}$, on the other hand, decays into $q\bar{q}\bar{\gamma}$ when it reaches its mass shell, and thus has always enough energy to give off a $b\bar{b}$ pair.

The study also covered the dependence of the results on the masses of the top quark and the gluino. We studied the events for top-quark masses of 43, 60, and 75 GeV, while the gluino's mass is varied for each top-quark mass (see Table I for details). In order to see how sensitive the results are to the scalar-quark masses, we varied them (see Table I), keeping them heavy enough that they are not created in the $\tilde{g}$'s decay. The idea behind this is the possibility[3] that the scalar-quark masses are higher

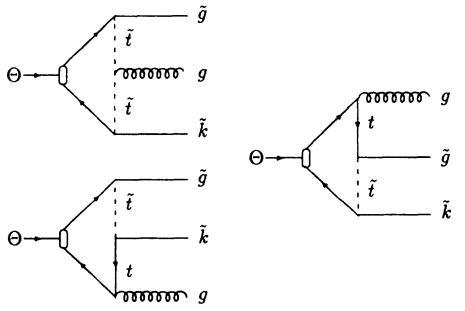

FIG. 1. The diagrams that contribute to $\Theta \to g\tilde{g}\tilde{k}$. $\tilde{k}$ can be either a $\tilde{g}$ or a $\bar{\gamma}$. The conjugate diagrams with $\tilde{k}$ and $\tilde{g}$ exchanged are not shown.

TABLE I. The various mass sets used in the study. Column 2 shows the scalar-quark masses, excluding the scalar top, which is shown in column 3. Column 4 shows the gluino's masses and column 5 shows the photino's masses. Column 6 shows the various top-quark masses used.

K_m Mass set	$m_{\tilde{q}}$ (GeV)	$m_{\tilde{t}}$ (GeV)	$m_{\tilde{g}}$ (GeV)	$m_{\tilde{\gamma}}$ (GeV)	m_t (GeV)
1	50	60	25	5	43
2	50	60	30	5	43
3	50	60	35	5	43
4	50	60	40	5	43
4a	200	200	40	5	43
5	100	100	60	5	43
6	80	100	70	5	43
7	65	65	40	5	60
8	65	65	45	5	60
9	100	100	50	5	60
9a	200	200	50	5	60
10	65	65	55	5	60
11	80	100	70	5	60
12	100	100	60	5	75
12a	200	200	60	5	75
13	100	100	65	5	75
14	80	100	70	5	75

than the gluino's mass. In some cases we distinguished between the $\tilde{t}$'s mass and the masses of the other scalar quarks. We assumed that the rest of the scalar quarks are mass degenerate.

Most of the figures in this paper show the results for $m_t = 60$ GeV, since the behavior of the events for the other mass sets is similar. We also show the results without normalization so we can see the actual number of events in a specific bin of a distribution. We must emphasize that although some of the mass sets were ruled out by the UA1 Collaboration,[8] the results depend explicitly only on the mass ratios, not on the masses themselves. Therefore, when the top-quark mass will be known, we will be able to identify in a more precise way the SUSY modes and, hopefully, the $\tilde{g}$'s mass.

In Sec. V we present the cross sections for the SUSY processes and their branching ratios. We also address the issue of how many events are expected in different colliders, including the Superconducting Super Collider (SSC).

The last point to be made is that although no one has proved, for the SUSY modes, the angle-ordering approach[9] in the cascade, it seems to be a reasonable way to proceed. The only place where we use this assumption, is for the radiation of gluons by the $\tilde{g}$'s. From the study, it appears that the $\tilde{g}$'s emit only a few gluons before reaching their mass shell and decay. After the decay, the ordinary cascade takes place, as will be described in the next section.

II. THE MONTE CARLO PROGRAM

The starting point in the study was the successful[5] coherent branching program EARWIG, which was written by Webber and Marchesini.[4] In order to include SUSY in Webber's program, a great deal of modification had to be done. Let me summarize this briefly.

First, the SUSY vertex probabilities had to be calculated.[10] Based on the above, the Sudakov form factors for the SUSY vertices were calculated giving us the probabilities that each particle will reach the next vertex at a certain energy. The procedure is discussed in Ref. 4. Having done that, the next step was to calculate the matrix element squared for the process, and embed it in the program.

Perhaps the most complicated modification to Webber's program was the insertion of the $\tilde{g}$ decay. This is a three-body decay (see Fig. 2) with a virtual $\tilde{q}$ as a propagator. The normal method used by Webber for the cascade was disrupted due to the virtuality of the $\tilde{q}$. The modification also had to preserve the original orientation of the plane of the decay in the $\tilde{g}$'s rest frame with respect to the momentum of the moving $\tilde{g}$.

Another problem that we encountered was the fact that Webber wrote his original program for a two-jet event with a possibility to emit a soft gluon as a third jet. The fact that the cascade is done in the infinite-momentum frame, caused the events to be highly collinear. We expected that since there is a lot of missing

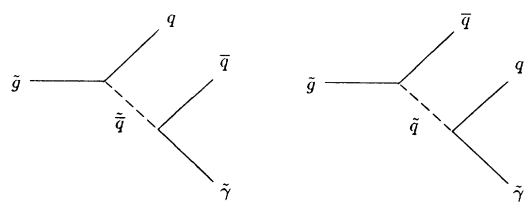

FIG. 2. The diagrams that contribute to the $\tilde{g}$ decay. The $\tilde{q}$ represents both left- and right-handed scalar quarks. The quarks may run over all possible flavors such that the decay is kinematically allowed.

energy in our case, the events will not necessarily be either collinear or planar. We therefore, had to preserve the original orientation of the decay plane of the Θ with respect to the boost which takes the Θ into the infinite-momentum frame.

A different problem that occurred in the modified program, was the fact that we treated the $\tilde{g}$ and $\bar{\tilde{g}}$ as different particles, ignoring the fact that they are Majorana particles. The purpose of the distinction between the two was to keep track of the fermion line and the color index (the hadronization model depends on the color lines) in the cascade. This ultimately created a slight spatial asymmetry between jets that originated from the $\tilde{g}$ and its antiparticle. The source of the asymmetry is embedded in the way Webber creates the third jet in his program. He basically emits the gluon from only one of the two fermions and checks to see if the energy is distributed according to the matrix element squared. The gluon then had a tendency to be closer to the $\tilde{g}$. Our solution was to randomize the origin of the gluon.

For the process $\Theta \rightarrow gg\gamma$, we use the same energy distribution as for $\Theta \rightarrow ggg$, i.e.,

$$\frac{1}{\Gamma}\frac{d^3\Gamma}{dx_1 dx_2 dx_3}(\Theta \rightarrow gg\gamma) = \frac{1}{\Gamma}\frac{d^3\Gamma}{dx_1 dx_2 dx_3}(\Theta \rightarrow ggg) ,$$

where x_i are the energy fractions of the decay products.

In the final step of the program we create jets from the final-state hadrons. We excluded the leptons from the jet definition. The jets are in a cone of $\sim 57°$. We did not vary this angle. We also excluded jets with energy less than 6 GeV in the jet analysis.

To conclude this section, we must emphasize that although many changes have been made in the original Webber program, the Monte Carlo method is the same and, more important, the hadronization method is the same. The program is still in the same "spirit" of its creator. It can carry out the original processes without any change.

III. THE EVENT'S SHAPE

The events that were produced by the Monte Carlo program give us a lot of information about what we expect to see in the colliders. The most prominent signature of these events is the huge amount of missing energy that is carried away by the photinos. The distribution of the missing energy and related quantities will be discussed in the following sections. Let me first start by examining some shape parameters, in order to get some idea of how the events will look.

A. The aplanarity and the sphericity measures (Ref. 11)

The frame that is used in studying the events is determined by the thrust axis. We first find the momentum tensor of all the observable particles, and calculate its eigenstates and eigenvalues. The particles are then rotated to the frame in which the axis (xyz) are the eigenstates of the momentum tensor with z as the major axis and x as the minor axis. If we denote the eigenvalues by Q_1, Q_2, Q_3, we can define the following quantities in terms of the Q's:

$$\text{aplanarity} \quad A = \tfrac{3}{2}Q_1 ,$$

$$\text{sphericity} \quad S = \tfrac{3}{2}(1 - Q_3) .$$

By looking at the aplanarity A (see Fig. 3), one can tell that all of the events are very planar. The $\Theta \rightarrow ggk$ mode is more planar than the $\Theta \rightarrow g\tilde{g}\tilde{k}$ mode. This is due to the fact that the latter has a secondary three-body decay ($\tilde{g}$ decay), which emits a $\tilde{\gamma}$ that does not participate in determining the momentum tensor.

The sphericity S (Fig. 4), however, indicates that although the events are planar, they are not confined to one axis. The two parameters must be read simultaneously in order to understand the spatial distribution of the event.

It is perhaps surprising that the $g\tilde{g}\tilde{k}$ mode is still rather planar. Even more surprising, the $g\tilde{g}\tilde{g}$ mode becomes more planar as the $\tilde{g}$'s mass increases. Let us understand in detail why this is the case.

We start by defining the two angles α and β as

$$\alpha = \arctan\left[\frac{y}{z}\right], \quad \beta = \arccos\left[\frac{x}{(x^2+y^2+z^2)^{1/2}}\right] ,$$

where (x,y,z) is any vector in the coordinates that were defined above. If the event was on the y-z plane, the angle β would be exactly 90°, i.e., β measures how planar the event is. The angle α measures the spatial distribution within the plane. Figure 5 shows how the jets are distributed in β. We see that the ggk mode is much more planar than the $g\tilde{g}\tilde{k}$ one, yet, the latter is still rather planar.

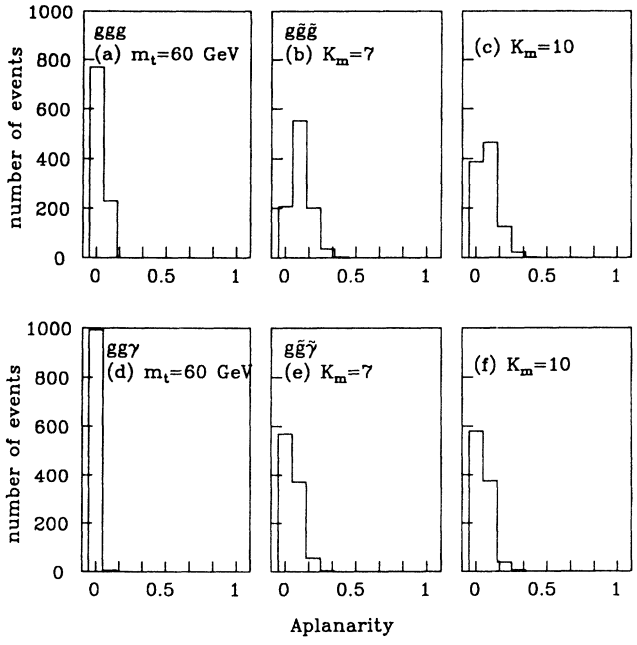

FIG. 3. The aplanarity A for $m_t = 60$ GeV. (a) for the ggg mode. (b) and (c) for $g\tilde{g}\tilde{g}$ mode (K_m refers to the mass set; see Table I). (d) for the $gg\gamma$ mode. (e) and (f) for $g\tilde{g}\tilde{\gamma}$ mode.

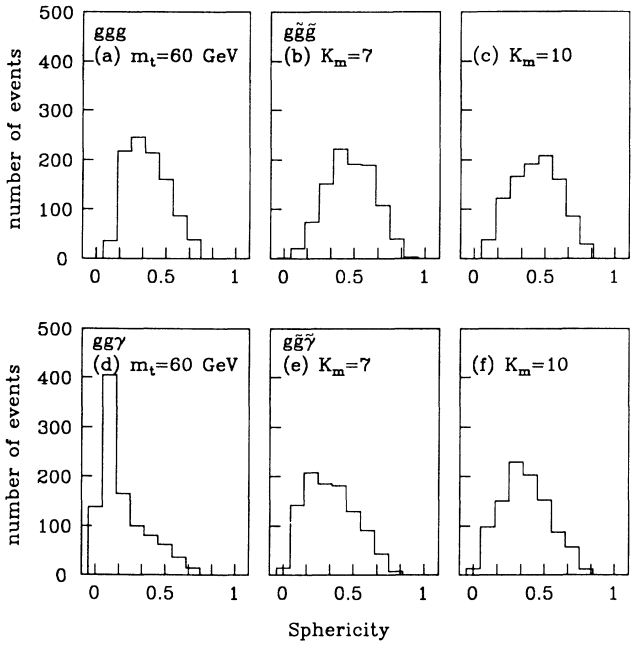

FIG. 4. The sphericity S. (a)–(f) vary in the same way as in Fig. 3.

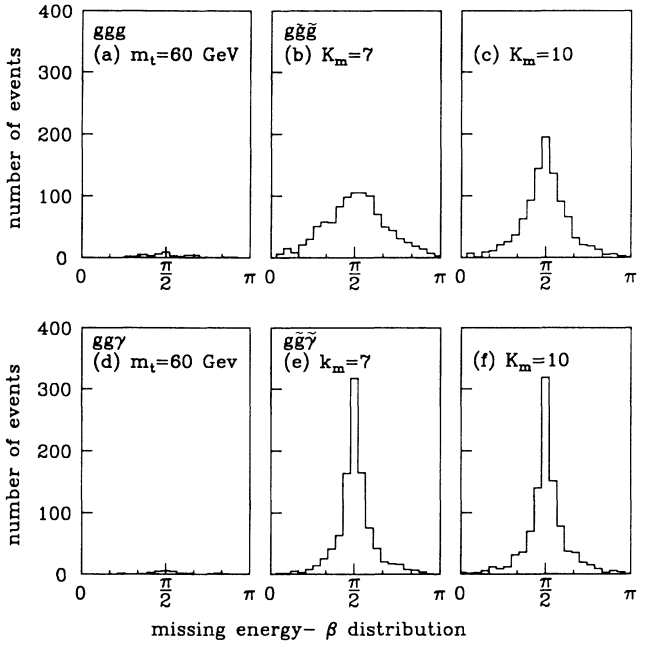

FIG. 6. The β distribution for the missing energy. (a)–(f) vary in the same way as in Fig. 3.

Figure 6, on the other hand, shows the β distribution of the missing energy, which is basically the sum of the two $\tilde{\gamma}$'s. Since we are in the rest frame of the Θ, the momentum of the missing energy should sum up (in the opposite direction) to the total momentum of the hadrons, i.e., the jets. Thus, the missing energy gives us a measure of how well the event's plane is defined. We clearly see that the missing energy, for the $g\tilde{g}\tilde{g}$ mode, is more confined to $\beta=90°$ as the $\tilde{g}$'s mass increases. This effect needs special attention.

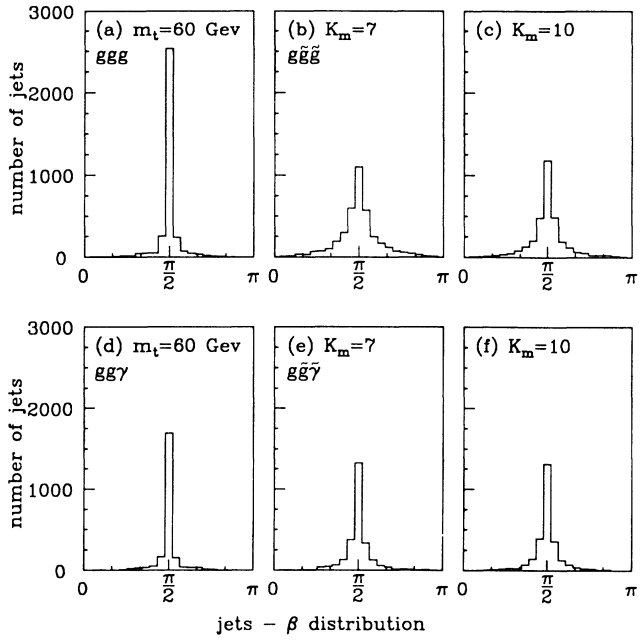

FIG. 5. The β distribution for jets. (a)–(f) vary in the same way as in Fig. 3.

The $\tilde{g}$ decays through an intermediate heavy scalar quark (Fig. 2). Because of the fact that there is a pole in the scalar-quark propagator, the invariant mass of the quark (or antiquark) and the $\tilde{\gamma}$, which come off the virtual scalar quark, is much larger than that of the $q\bar{q}$ pair [we did not observe any significant change in this behavior when we varied the mass of the scalar quark (see Table I)]. Thus, in the rest frame of the $\tilde{g}$, its decay products tend to come out collinear.

When the $\tilde{g}$'s mass is close to the top-quark mass, the two $\tilde{g}$'s are rather slow and come out in opposite direction, while the gluon is almost at rest (Fig. 7). Each $\tilde{g}$ then decays, but its decay products are confined to an axis. Thus, the products of the two $\tilde{g}$'s create a well-defined plane, which is the event's plane. When the $\tilde{g}$'s mass decreases, the gluon is harder, and the decay products of each $\tilde{g}$ come out within a cone that can acquire large angles (depends on how fast the $\tilde{g}$ moves). The event's plane is then not so well defined, and the missing energy is no longer confined to the event's plane. The fact that the jets (Fig. 5) have different β distribution than the missing energy, is because we enter ~ 3 times as many jets as the missing energy, in each bin of the distribution.

In the $gg\tilde{\gamma}$ mode, however, the event's plane is well defined, and the missing energy is confined to the event's plane no matter what the $\tilde{g}$ mass is. This time the missing-energy three-momentum consists mainly of the momentum of the $\tilde{\gamma}$ that comes off the Θ. The gluon is also hard (Fig. 8) and is very important in determining the event's plane. The $\tilde{g}$ comes out fast enough that its

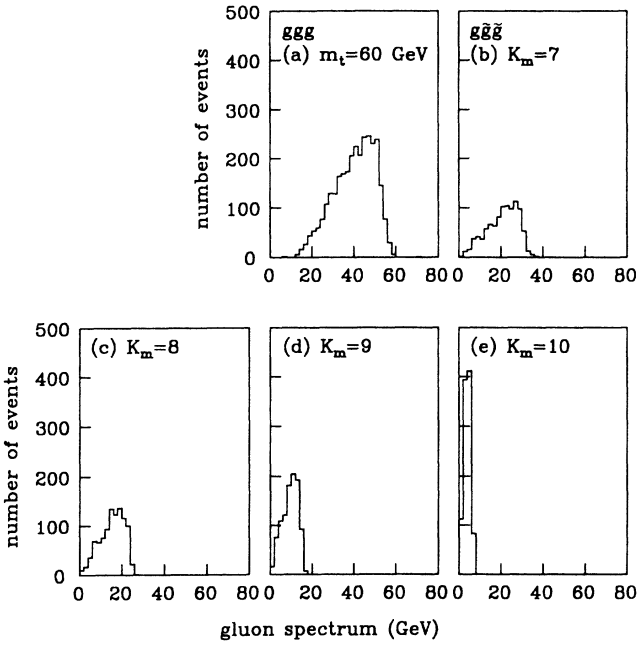

FIG. 7. Gluon spectrum (GeV) for $m_t = 60$ GeV. (a) for ggg mode. (b)–(e) show progression as the $\tilde{g}$ mass increases for the $g\tilde{g}\tilde{g}$ mode.

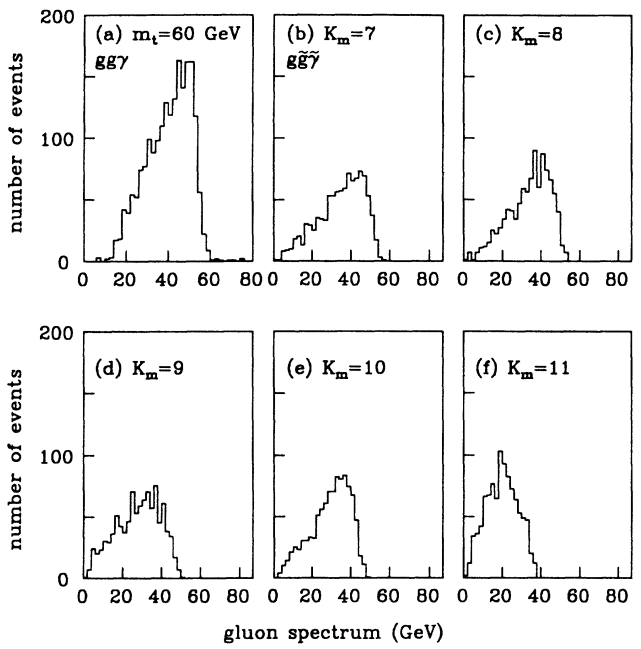

FIG. 8. Gluon spectrum (GeV) for $m_t = 60$ GeV. (a) for $gg\gamma$. (b)–(f) show progression as the $\tilde{g}$ mass increases, for $g\tilde{g}\tilde{\gamma}$ mode.

decay products lie within a narrow cone.

Another important tool to understand the event's shape is the Fox and Wolfram method, as will be described next.

B. The Fox and Wolfram shape parameters (Ref. 12)

Let us define the harmonic moments H_l as follows:

$$H_l = \sum_{i,j} \frac{|\mathbf{p}_i||\mathbf{p}_j|}{s} P_l(\cos(\phi_{i,j})) \ .$$

I treat the total missing energy as one four-vector. If all the final-state particles were massless, H_0 would be 1. If the three-momentum of the final state were zero, i.e., momentum conservation in the Θ rest frame, H_1 would vanish. We can expect a deviation from unity in H_0 since it is obvious that most of the particles are massive, but no deviation in H_1 from zero should occur.

The results verify that $H_1 = 0$ in all cases. H_0 (Fig. 9), on the other hand, is far from 1 for the SUSY mode $\Theta \to g\tilde{g}\tilde{k}$, but is very close to 1 for $\Theta \to ggk$. This can serve to distinguish between the two modes. There are two main reasons for this difference.

(i) The missing energy in $\Theta \to g\tilde{g}\tilde{k}$ is larger than in $\Theta \to ggk$, and is carried away by the $\tilde{\gamma}$'s, which have mass (in contrast with the ν's which are the only carriers of the missing energy in the $\Theta \to ggk$ mode). The dominant effect, however, comes from the fact that the total missing energy-momentum vector is treated as one "particle" in evaluating the H_l. Since there are two $\tilde{\gamma}$'s in each SUSY mode, the combined four-vector can acquire a large mass. The results show that the combined mass can be as heavy as the total missing energy itself.

(ii) In the $\Theta \to ggk$ mode the outcoming particles consist mainly of π's, i.e., light particles, while in the $\Theta \to g\tilde{g}\tilde{k}$ mode we see more B hadrons in the jets. (This will be discussed later on in more detail.)

The other three moments that were studied, H_2, H_3, and H_4, do not seem to give any new information about the event's shape. In the $k = g$ case, we notice that H_2

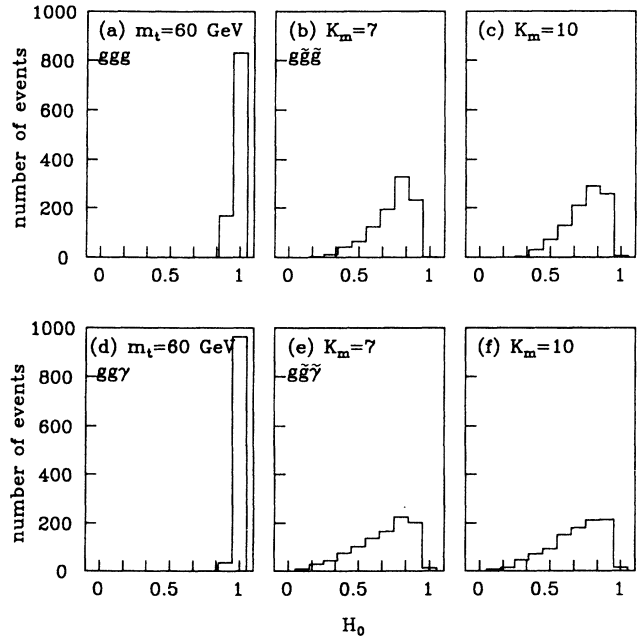

FIG. 9. Fox and Wolfram parameter H_0. (a)–(f) vary in the same way as in Fig. 3.

and H_3 become a bit harder as the $\tilde{g}$'s mass increases. This is in full agreement with the observation that the events have higher thrust as the $\tilde{g}$'s mass increases. The effect, though, is very small. H_4, on the other hand, does not change for all the different mass sets. In the $k=\gamma$ case the above effect is more prominent.

Perhaps the most interesting thing about the H_l's in the SUSY modes of the Θ decay, is the remarkable resemblance to the heavy-quark and -lepton production events that were studied by Fox and Wolfram.[12] The analogy is very clear. In both cases we have heavy fermions decaying through a heavy exchange particle into quarks which ultimately produce jets. This resemblance indices that the g's jet is rather soft in the Θ decay. The $gg\tilde{g}$ mode looks more like heavy-lepton production, while the $gg\tilde{\gamma}$ mode looks like heavy-quark production. This is obvious since in the $gg\tilde{\gamma}$ mode we have an extra hard gluon jet. The difference between our events and those of Fox and Wolfram is in the amount of missing energy, as will be discussed later.

C. Jet analysis

In most papers written on the process $\Theta\rightarrow g\tilde{g}\tilde{k}$ it is predicted that the event will have two or three jets, depending on whether the $\tilde{k}$ is a photino or a gluino. The assumption was that the gluino creates its own jet. From the Monte Carlo calculation it appears that the gluino by itself is not the direct "father" of the jet, rather, its offspring (i.e., the quarks that come from its decay) produce jets. Since the two different processes have a unique signature, let us analyze each one separately.

1. $\Theta\rightarrow ggg$

From Fig. 10 we can see that the process $\Theta\rightarrow ggg$ consists mostly of three-jet events. As the top mass increases the number of four-jet events increases as well as the number of five-jet events, although the latter is still negligible. No monojet events were registered in the above process. This result is well understood. As the top mass increases the three gluons come out with higher energy; thus, the probability of emitting a hard gluon in the beginning of the cascade, is higher. The hard gluon ultimately creates its own jet.

On the other hand, in the case of $\Theta\rightarrow gg\tilde{g}$ we see (Fig. 11) that the number of four- and five-jet events is abundant, even at lower top mass. The interesting fact is that the number of four-, five-, and six-jet events decreases as the gluino's mass increases. The reason for this effect is that the energy of the original gluon decreases as the gluino's mass increases, thus the number of jets that are related to the gluon decreases. We can see this by looking at the energy spectrum of the original gluon and the quarks that come from the gluino's decay, in comparison to the jet spectrum (Figs. 7, 12, and 13). The jet spectrum resembles that of the quarks and not that of the gluon. Notice the existence of monojets [there is one in Figs. 11(a) and 11(b), two in Fig. 11(c) and 12 in Fig. 11(d)]. I will not discuss them in this paper since they were widely analyzed in various papers.

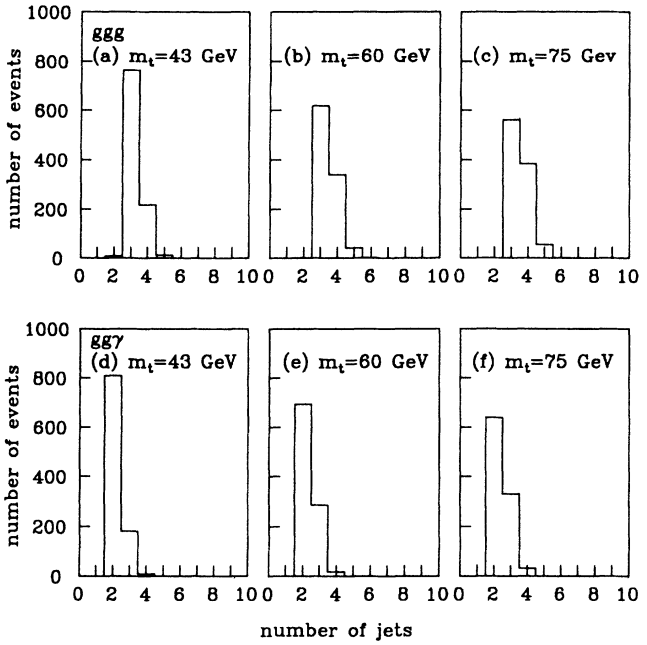

FIG. 10. Number of jets. (a)–(c) show progression as the top-quark mass increases for the ggg mode. (d)–(f) the same, but for $gg\gamma$ mode.

If we look more carefully at the peak of the jet's spectrum, we note that it shifts to higher energies as the $\tilde{g}$'s mass increases, yet, the upper limit of the jet energy spectrum is constant with respect to the $\tilde{g}$'s mass. It appears that the latter falls very close to the top mass. In this paper we assume that the top mass is known, thus the above parameter can serve as a test for it.

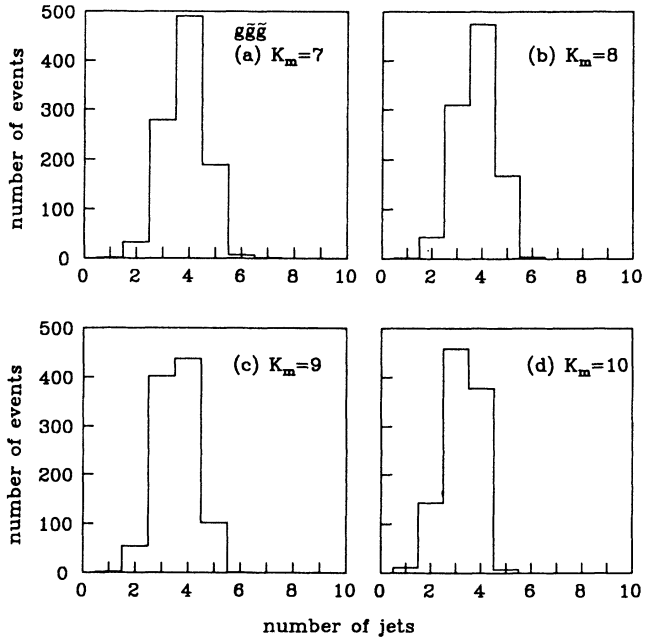

FIG. 11. Number of jets for $m_t=60$ GeV. (a)–(d) show progression as the $\tilde{g}$ mass increases for the $gg\tilde{g}$ mode.

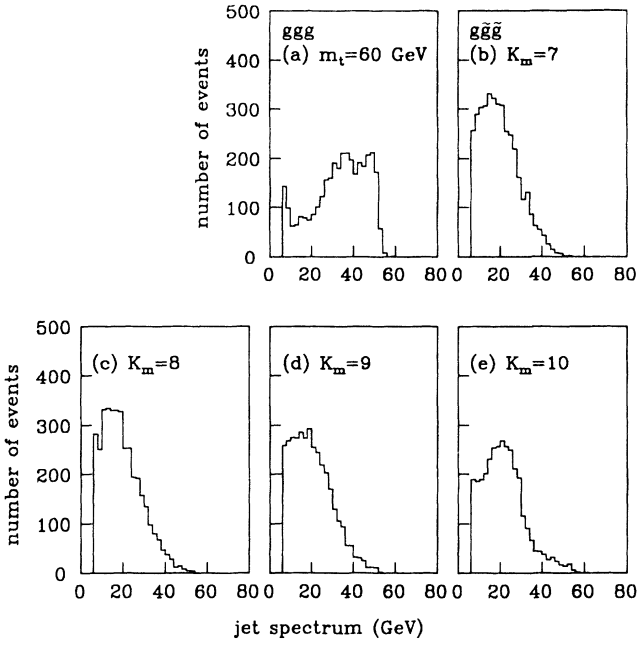

FIG. 12. Jet spectrum (GeV) for $m_t=60$ GeV. (a) for ggg mode. (b)–(e) show progression as the $\tilde{g}$ mass increases for the $gg\tilde{g}$ mode.

The jet's mass distribution, in the $\Theta\rightarrow gg\tilde{g}$ mode, does not change with the $\tilde{g}$'s mass for a certain top mass, but seems to have a higher maximum value as the top mass increases. The peak of the distribution stays at about the same value. The jet's mass in the $\Theta\rightarrow ggg$ mode, on the other hand, peaks at higher values, but stays within the same range as in the SUSY mode.

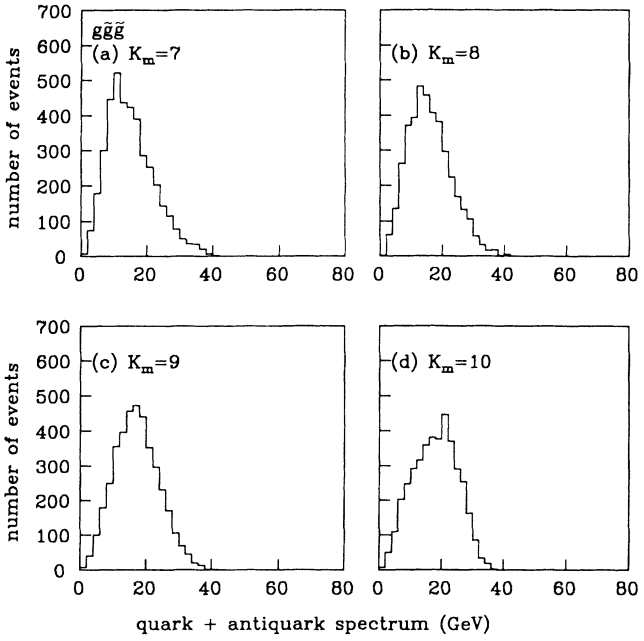

FIG. 13. $q\bar{q}$ spectrum (GeV). For each event we entered the energy of the quark and the antiquark separately. (a)–(d) vary in the same way as in Fig. 11.

Another important variable is the hadron multiplicity in the jet. We can see a distinct feature of the $\Theta\rightarrow ggg$ mode (Fig. 14). The difference between the modes comes, again, from the jet origin. In the $\Theta\rightarrow ggg$ mode all the jets are related to the gluons. The gluons are color octet and therefore create more particles in a jet than quarks. From the charged-particle multiplicity we see that most of the particles in the jets are charged. The jets, on the other hand, are mostly neutral.

2. $\Theta\rightarrow gg\tilde{\gamma}$

An analysis of this process was performed by Buchmüller, Kuhn, and Martin,[13] in which they show the missing energy spectrum using a different Monte Carlo method for one set of masses ($m_t=m_{\tilde{t}}=40$ GeV, $m_{\tilde{g}}=60$ GeV, $m_{\tilde{\gamma}}=0$). Our result basically agrees with what they found. Here we present a number of additional properties of the events, not discussed in Ref. 13.

By looking at the number of jets in the process $\Theta\rightarrow gg\gamma$ (Fig. 10) one can see the two-jet feature of the event. As in the process $\Theta\rightarrow ggg$, the same effect of increasing number of three- and four-jet events can be noticed, as well as no monojet events. Yet, in the process $\Theta\rightarrow gg\tilde{\gamma}$ (Fig. 15) we start to see some different features. First, the number of monojets is quite substantial for all mass ratios. Second, one notices that as the gluino's mass increases beyond the top mass, the two-jet events become more significant. This is due to the fact that the gluon does not give hard jets (one can see that from the jet spectrum, Fig. 16). As in the previous case, the quarks that come from the decay of the gluino are the ones responsible for the jets. The gluon only explains the "bump" in the higher tail of the distribution, when the $\tilde{g}$'s mass is

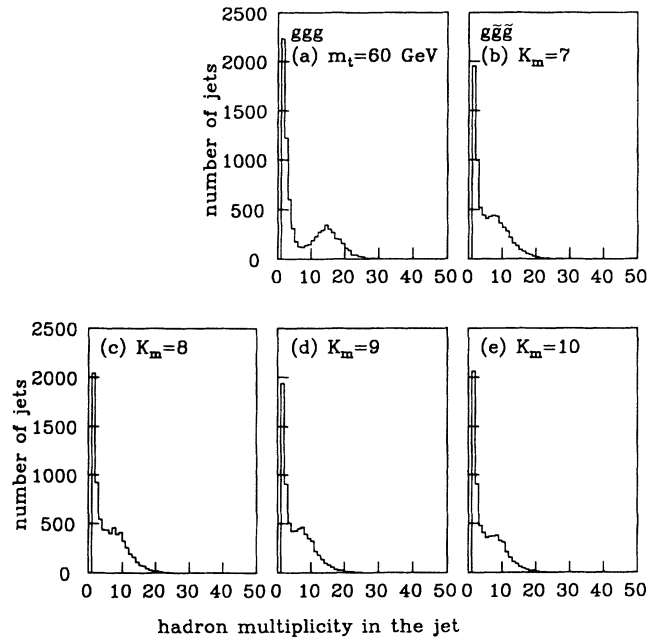

FIG. 14. Hadron multiplicity in the jet. (a)–(e) vary in the same way as in Fig. 12.

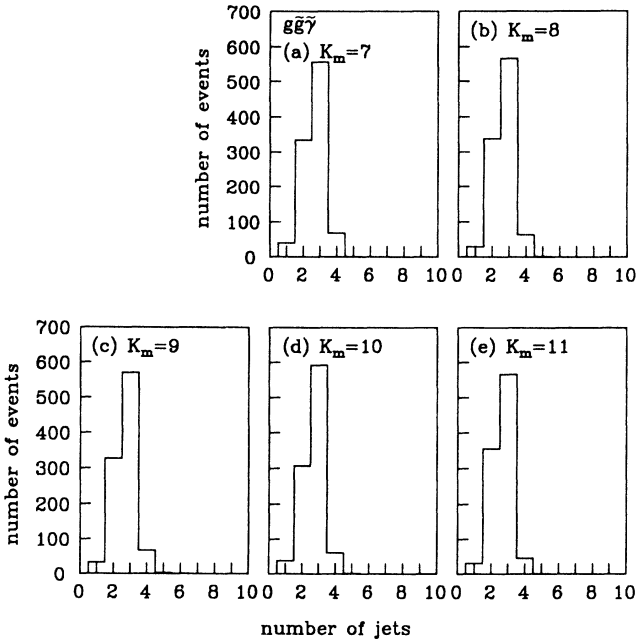

FIG. 15. Number of jets for $m_t = 60$ GeV. (a)–(e) show progression as the $\tilde{g}$ mass increases for the $g\tilde{g}\tilde{\gamma}$ mode.

small. As we shall see later, the missing energy in this process is the most striking feature. The events seem also to be much more planar than the previous case. This is obvious, since now, only one gluino exists.

The jet's spectrum (Fig. 16), behaves like the previous case, with its maximum near the top mass. The jet's multiplicity also resembles the previous case, again, indicating that although the gluon is harder, most of the jets come from the quarks.

D. The jet's composition

As mentioned before, the leptons were excluded from the jet's definition. The hadrons which form the jets, consist mainly of π's, η's, and K's. There are a few baryons and photons in each event.

Perhaps the most interesting component in the jets are the B hadrons. In Fig. 17 we see that there are many more B particles in the SUSY decay modes than in the ordinary case. This is because of the relatively high probability for the b quarks to be produced at the primary $\tilde{g}$ decay vertex. This result is similar for the $g\tilde{g}\tilde{\gamma}$ mode.

It appears that the B multiplicity increases as the top mass increases, for the $\Theta \rightarrow ggk$ mode. This is expected since we get harder gluons from the heavier Θ. By contrast, the B multiplicity decreases as the $\tilde{g}$'s mass increases (Fig. 17), for the $\Theta \rightarrow g\tilde{g}\tilde{k}$ mode [it changes between a total number of 556 B's in Fig. 17(b), to 502 in Fig. 17(e). In the $g\tilde{g}\tilde{\gamma}$ mode we also see a drop of $\sim 10\%$ in the B multiplicity]. The only reason that this can happen is that $\sim 10\%$ of the B's come from the gluon, when the $\tilde{g}$'s mass is small, which verifies our expectation that most of the B's will come from the $\tilde{g}$'s. As the $\tilde{g}$'s mass increases the g becomes softer and has less chance to give off a heavier quark pair. The B spectrum, on the other hand, peaks at higher energies as the $\tilde{g}$'s mass increases, but remains within the same limits. The behavior for the case $k = \gamma$ is similar to that of $k = g$ in both spectrum and multiplicity. The only difference is that the number

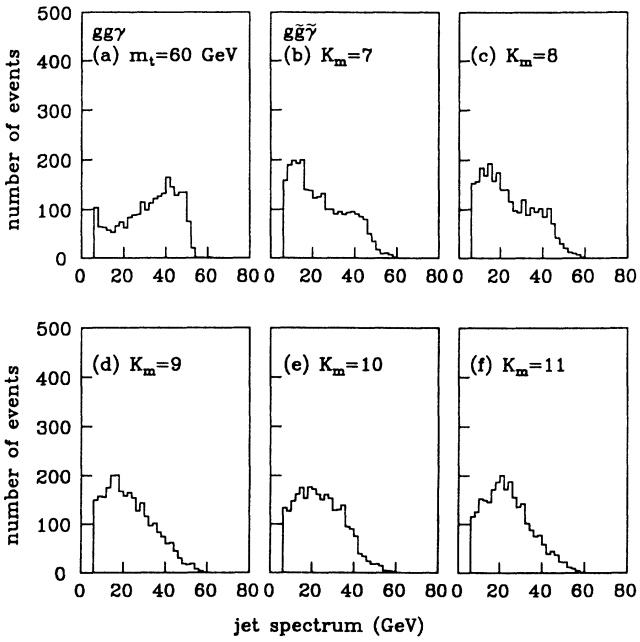

FIG. 16. Jet spectrum (GeV) for $m_t = 60$ GeV. (a) for $gg\gamma$ mode. (b)–(f) show progression as the $\tilde{g}$ mass increases, for the $g\tilde{g}\tilde{\gamma}$ mode.

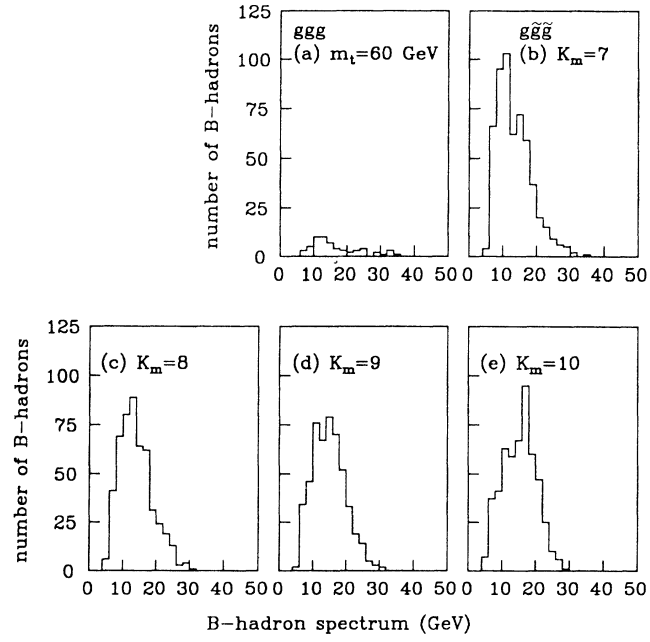

FIG. 17. B-hadron spectrum (GeV) for $m_t = 60$ GeV. (a) for ggg mode. (b)–(e) show progression as the $\tilde{g}$ mass increases for the $g\tilde{g}\tilde{g}$ mode.

of B's is less by $\sim 40\%$ to 50% for $k=\gamma$, due to the fact that we have only one $\tilde{g}$, in comparison to two in the $k=g$ case.

Another important component of the jets are the D mesons. In my program the charm quark's decay was turned on. The way to recognize it is by looking at the weak decays into leptons. We observed that the number of ν's increases dramatically in the SUSY modes (by a factor of 3 to 5). The number of μ's also becomes significant for the SUSY modes. We must emphasize that all the weak decays were channeled through the W. No $Z^0 \rightarrow l\bar{l}$ occurred. Thus, the total number of ν's equals that of the charged leptons.

IV. THE MISSING ENERGY

When we compare the missing-energy distributions of the $\Theta \rightarrow g\tilde{g}\tilde{k}$ to the $\Theta \rightarrow ggk$, it is evident (Figs. 18 and 19) that one can put a cut on the curve at ~ 20 GeV in order to distinguish between the two processes. The $\Theta \rightarrow ggk$ process did not exceed 20 GeV in missing energy. Further, the distribution peaks at only a few GeV, in most cases.

In the SUSY mode $\Theta \rightarrow g\tilde{g}\tilde{k}$ the missing energy distribution peaks at much higher energies. One can see that as the $\tilde{g}$'s mass increases, in $\Theta \rightarrow g\tilde{g}\tilde{g}$, the peak of the distribution is shifted towards higher energies. This is expected since each $\tilde{g}$ gets higher energy, thus has higher probability to emit harder $\tilde{\gamma}$. Nevertheless, the maximum missing energy $E_{\text{miss}}^{\max}$ decreases with the $\tilde{g}$'s mass. As we will see later, it is highly correlated to the $\tilde{\gamma}$'s energy.

In the $\Theta \rightarrow g\tilde{g}\tilde{\gamma}$ case there seems to be no significant change in the missing energy distribution, as the $\tilde{g}$'s mass

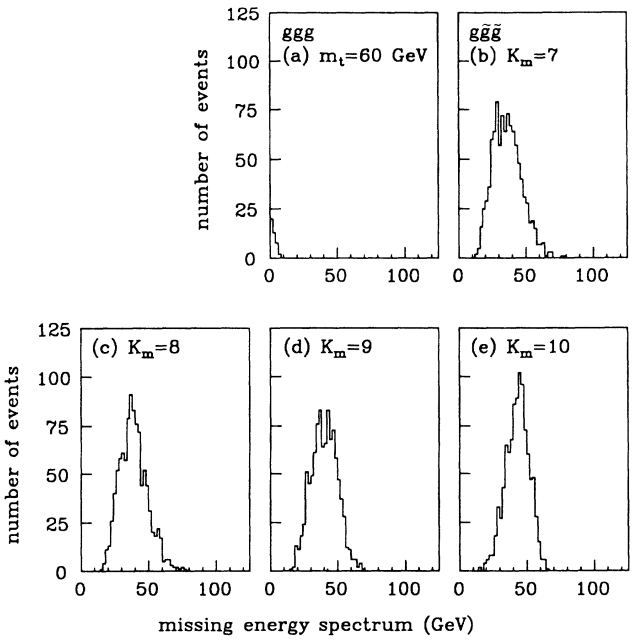

FIG. 18. Missing-energy spectrum (GeV). (a)–(e) vary in the same way as in Fig. 17.

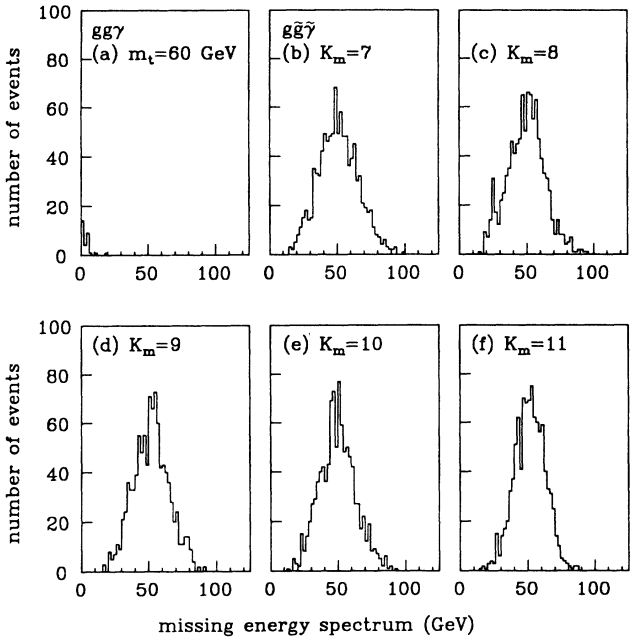

FIG. 19. Missing-energy spectrum (GeV). (a)–(f) vary in the same way as in Fig. 16.

increases. This can be explained by the following argument: As the $\tilde{g}$'s mass increases, the $\tilde{\gamma}$ that comes directly from the Θ gets less energy, while the $\tilde{\gamma}$ that comes from the $\tilde{g}$'s decay gets higher energy. On the average, the two effects cancel, and the distribution remains unchanged. On the other hand, when the $\tilde{g}$'s mass exceeds the top mass, the higher tail of the distribution shrinks, while the peak remains on the same energy. This indicates that the $\tilde{\gamma}$ that comes from the Θ is the one which is responsible for the higher-energy tail of the distribution. If we compare the $\Theta \rightarrow g\tilde{g}\tilde{g}$ distribution to that of $\Theta \rightarrow g\tilde{g}\tilde{\gamma}$, we see that the latter peaks at higher energies when the $\tilde{g}$'s mass is small compared to the top mass. As the $\tilde{g}$'s mass increases, the peak is on the same energy, yet, the $g\tilde{g}\tilde{g}$ mode has narrower distribution; i.e., the higher tail shrinks. This can help to distinguish between the two processes. In both modes there was no effect of the mass of the scalar quark (see Table I), which mediates the $\tilde{g}$ decay, on the missing-energy distribution.

Let me show now how the missing-energy distribution can be used to calculate the mass of the $\tilde{\gamma}$ and the $\tilde{g}$.

A. The masses of the photino and the gluino (Ref. 14)

The missing-energy distribution can be used as an important tool to predict both the $\tilde{\gamma}$ and the $\tilde{g}$ masses. The basic idea here is the fact that the maximum energy of each $\tilde{\gamma}$, $E_{\tilde{\gamma}}^{\max}$, in the Θ rest frame, is a unique function of the $\tilde{g}$'s mass (as will be shown later in this section). We therefore want to correlate the maximum missing energy $E_{\max}^{\text{miss}}$ to $E_{\tilde{\gamma}}^{\max}$ since the former is an observable parameter. The result can then be checked (see the Appendix) by calculating how many events are expected to have the

observed $E_{\max}^{\text{miss}}$, using the calculated $\tilde{g}$ mass. It is obvious that the latter can only be applied if we have enough events to actually perform statistical analysis. This issue will be addressed in the next section. Let us develop the method in detail.

The minimum of the missing energy distribution can be used as a rough indication of the $\tilde{\gamma}$ mass; averaging over the minima of the distributions in Figs. 18(b)–18(e) and Figs. 19(b)–19(f) we get

$$E_{\min}^{\text{miss}} \approx (2.92 \pm 0.57) m_{\tilde{\gamma}} \quad (\Theta \to g\tilde{g}\tilde{g}) ,$$

$$E_{\min}^{\text{miss}} \approx (3.46 \pm 0.60) m_{\tilde{\gamma}} \quad (\Theta \to g\tilde{g}\tilde{\gamma}) .$$

The error ($\sim 20\%$) indicates that we can use the latter only as a rough estimate to the $\tilde{\gamma}$'s mass. In our next calculations we assume that $E_{\min}^{\text{miss}} = 2m_{\tilde{\gamma}}$, since this is the theoretical prediction, knowing that the above is only an upper limit to the $\tilde{\gamma}$ mass. We found that $m_{\tilde{\gamma}}$ has little effect on the results, due to the fact that $E_{\tilde{\gamma}}^{\max}$ depends quadratically on the ratio $Y \equiv m_{\tilde{\gamma}}/m_{\tilde{g}}$.

The maximum missing energy can give us a very good estimate of the $\tilde{g}$ mass, only in the process $\Theta \to g\tilde{g}\tilde{g}$, but not for $\Theta \to g\tilde{g}\tilde{\gamma}$, due to the fact that the energy distribution, in the latter, does not change much, as was described previously.

In order to get the absolute maximum of the missing energy we make the following assumptions.

(i) The maximum missing energy will come from those events for which the gluon is very soft. Let us assume, for the moment, that the gluon's energy is negligible, thus each gluino has the energy $E_{\tilde{g}} \simeq m_t$.

(ii) The $\tilde{g}$ decays before emitting any gluons. In the rest frame of the $\tilde{g}$, the maximum energy that the $\tilde{\gamma}$ can acquire is

$$(E_{\tilde{\gamma}}^{*})^{\max} = \frac{m_{\tilde{g}}^2 + m_{\tilde{\gamma}}^2}{2m_{\tilde{g}}} . \tag{4.1}$$

The maximum energy of the $\tilde{\gamma}$ in the Θ rest frame is

$$E_{\tilde{\gamma}}^{\max} = \gamma[(E_{\tilde{\gamma}}^{*})^{\max} + \beta(P_{\tilde{\gamma}}^{*})^{\max}] , \tag{4.2}$$

where

$$P_{\tilde{\gamma}}^{*} = [(E_{\tilde{\gamma}}^{*})^2 - m_{\tilde{\gamma}}^2]^{1/2}$$

and

$$\gamma = \frac{E_{\tilde{g}}}{m_{\tilde{g}}} \simeq \frac{m_t}{m_{\tilde{g}}}, \quad \beta = \frac{P_{\tilde{g}}}{E_{\tilde{g}}} = (1 - 1/\gamma^2)^{1/2} .$$

The maximum $\tilde{\gamma}$ energy can now be written, using all of the above, as

$$E_{\tilde{\gamma}}^{\max} = \frac{m_t}{2}[1 + Y^2 + \beta(1 - Y^2)] . \tag{4.3}$$

Fixing the top mass m_t, $E_{\tilde{\gamma}}^{\max}$ is a unique function of the $\tilde{g}$ mass. As shown in Fig. 20, there is a very strong, linear correlation between $E_{\tilde{\gamma}}^{\max}$ and $(E_{\tilde{\gamma}}^{miss})_{\max}$, the total energy that is carried away by both photinos. The fit is

$$(E_{\tilde{\gamma}}^{\text{miss}})_{\max} = aE_{\tilde{\gamma}}^{\max} + b \tag{4.4}$$

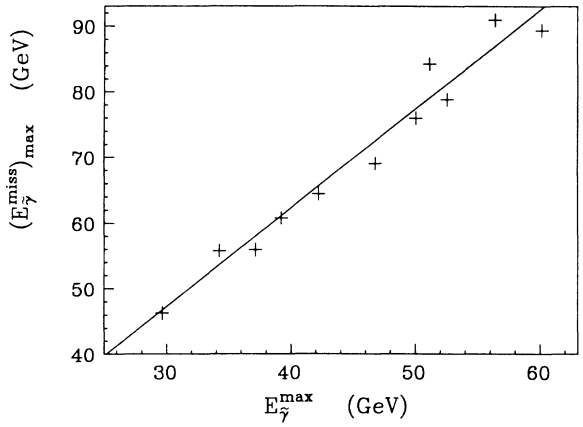

FIG. 20. $(E_{\tilde{\gamma}}^{\text{miss}})_{\max}$ vs $E_{\tilde{\gamma}}^{\max}$ in GeV. The figure shows the strong linear correlation between the two.

with $a = 1.509 \pm 0.128$, $b = (2.033 \pm 4.489)$ GeV.

In the experiment we measure the absolute maximum of the missing-energy distribution, $E_{\max}^{\text{miss}}$, rather than $(E_{\tilde{\gamma}}^{\text{miss}})_{\max}$. We cannot tell how much missing energy is carried away by the ν's. One can only approximate $(E_{\tilde{\gamma}}^{\text{miss}})_{\max}$ by subtracting the total energy that the observable leptons carry, from $E_{\max}^{\text{miss}}$ (we found no relation between the energy carried away by the observable leptons to the energy carried away by the neutrinos). The analysis shows that the events that contribute to $E_{\max}^{\text{miss}}$ usually have no neutrinos.

Estimating $m_{\tilde{\gamma}}$ from $E_{\min}^{\text{miss}}$ we can solve for $m_{\tilde{g}}$ using Eq. (4.3). The top mass is taken to be $m_t = \sqrt{s}/2$. The results are shown in Table II.

The above method can be checked, by a more analytical approach, using the $\tilde{\gamma}$'s energy distribution (see the Appendix) in the Θ rest frame. We can calculate the branching ratio for the events that are expected to have the observed $E_{\max}^{\text{miss}}$, using the predicted value for $m_{\tilde{g}}$. If the result agrees with the experiment, then the predicted value can serve as a good estimator since the two methods are uncorrelated. Table II shows the result for the above procedure. We see that for the region where the fit (4.4) is good, the error in $m_{\tilde{g}}$ is small, indicating that our predicted value is good. In all cases, the predicted value is not off by more than 5 GeV. This is true even if we take into account the error due to energy mismeasurement. We found that an energy resolution of $\sigma(E)/E \sim 40\%/\sqrt{E}$ (where E is the total energy detected in an event, in GeV) in the hadronic calorimeters, will change the calculated mass of the $\tilde{g}$ by 2–4 GeV.

V. THE CROSS SECTIONS AND BRANCHING RATIOS

The discussion in this paper is relevant only if we will be able to see the SUSY modes in present or future colliders. The situation in e^+e^- machines does not seem to be very promising due to the fact that both the luminosities and the branching ratios are small. Table III shows the

TABLE II. The reconstruction of the $\tilde{g}$'s mass. Column 1 refers to the mass sets (see column 1 in Table I). Column 2 shows the input mass of the $\tilde{g}$, while column 3 shows the calculated one. Column 4 shows the branching ratios for the events that contribute to the observed maximum missing energy in $\Theta \rightarrow g\tilde{g}\tilde{g}$ (see Fig. 18). A value of 10^{-3}, in our case, translates to the observed 1 event.

K_m (see Table I)	$m_{\tilde{g}}$ (Input) (GeV)	$m_{\tilde{g}}$ (Calculated) (GeV)	Branching ratio (10^{-3})
1	25	23.81±1.57	0.60
2	30	31.43±0.92	0.91
3	35	31.65±0.90	0.93
4	40	39.46±0.36	3.60
7	40	42.78±1.35	0.77
8	45	46.18±1.10	1.16
9	50	52.52±0.68	2.34
10	55	55.51±0.48	4.36
12	60	63.16±1.01	1.92
13	65	61.79±1.10	1.56
14	70	64.59±0.92	2.42

production cross sections at the CERN e^+e^- storage ring LEP. The reason for the small cross section is machine dependent[15] (the beam width is much larger than the Θ width). We also show in Table III the branching ratios for the SUSY modes. We must emphasize, though, that if the top-quark mass is $\sim$30 GeV, then the KEK storage ring TRISTAN will see the SUSY modes (probably only the $g\tilde{g}\tilde{\gamma}$ one) first, if kinematically allowed, due to the larger branching ratios and the large luminosity.

TABLE III. The branching ratios for $\Theta \rightarrow g\tilde{g}\tilde{k}$ and the expected size for Θ production in various colliders. The production cross section at LEP was calculated using an expected energy spread (Ref. 15) of $\delta E_{\rm LEP} \simeq [4.4\times10^{-3}s\ ({\rm GeV}^2)]$ MeV. The production at SSC was taken from Ref. 15 for $\sqrt{s}=40$ TeV.

K_m	Branching ratio ($\Theta \rightarrow g\tilde{g}\tilde{g}$) ($10^{-5}$)	Branching ratio ($\Theta \rightarrow g\tilde{g}\tilde{\gamma}$) ($10^{-5}$)	Θ production (pb)
1	310	64	362
2	161	46	(at LEP)
3	57	32	(Ref. 15)
4	5.6	21	
4a	0.03	0.4	
5		0.6	
6		0.07	
7	177	42	105
8	100	32	(at LEP)
9	7.9	7.2	(Ref. 15)
9a	0.4	0.7	
10	8.5	16	
11		2	
12	9.2	4.6	15
12a	0.6	0.6	(at SSC)
13	3.3	3.9	(Ref. 16)
14	0.6	2.6	

The other alternatives are the hadron-hadron colliders. In these machines the main channel for the Θ production comes from the subprocess $gg \rightarrow \Theta g$, thus the signature is not as "clean" as in the e^+e^- colliders. In Ref. 16 we see that the production cross section is rather small. However, the luminosity in these machines can be as large as 10^{33} cm^{-2} sec^{-1} (SSC). Moreover, if one uses the Cornell[17] potential for the Θ bound state, one can get a production cross section which is larger by a factor of $\sim$10. This will put the SSC on a production level which will allow us to actually do statistics on the SUSY modes. For instance, using a production cross section of[15] 40 pb, at $\sqrt{s}=40$ TeV, $m_t=60$ GeV, $\mathcal{L}=10^{33}$ cm^{-2} sec^{-1} and a branching ratio of 7.9×10^{-5} ($m_{\tilde{g}}=50$ GeV for the $\Theta \rightarrow g\tilde{g}\tilde{g}$ mode), one gets $\sim$11 events over a period of 1000 h at the SSC. This can improve by a factor of 10 using the Cornell potential. The numbers are even more promising for some of the other mass sets that were used in this study (see Table III).

VI. CONCLUSION

From the Monte Carlo results it is obvious that supersymmetry, if it exists, leaves some remarkable signatures behind. First, assuming that R parity is conserved, the lightest SUSY particles can carry away a huge amount of missing energy. Second, the latest predictions for higher mass of the top quark give rise to events with larger numbers of jets. These multiple-jet events can be easily detected. The high number of B hadrons in the jets, together with the large amount of missing energy, can make it easier for us to detect SUSY.

An important outcome of the study is the fact that the jets do not originate from the $\tilde{g}$'s but from their offspring. This can be used to distinguish the SUSY modes from the non-SUSY mode of the Θ decay, since we have shown that the quark jets, in the SUSY modes, have a different spectrum than the gluon jets, in the non-SUSY modes. The fact that the gluon's jet is highly suppressed

in the SUSY mode, due to the high mass of the $\tilde{g}$, helps even more.

Since the Monte Carlo calculation depends on so many different SUSY particles, it might appear that all the different (and unknown) SUSY masses would influence the shape of the events. We find that there is no dependence on the masses of the $\tilde{q}$'s, which participate in the $\tilde{g}$'s decay (the mass of the $\tilde{t}$ is relevant only to the branching ratios of the SUSY modes), and the mass of the $\tilde{\gamma}$, assuming the latter to be light. This then reduces the number of important masses to two, the top quark and the $\tilde{g}$. In fact, the appearance of the events depends only on the ratio between the two masses. Assuming that the mass of the top quark will be known before SUSY can be detected, the $\tilde{g}$'s mass can be calculated using the method in Sec. IV A. If we do not know the mass of the top quark, and if SUSY does exist, we will then be able to see events with large peak of missing energy, at the toponium resonance. This, hopefully, will determine the masses of both the top quark and the $\tilde{g}$.

ACKNOWLEDGMENTS

This work was supported in part by Department of Energy Contract No. DEACO 276 ERO 1195 Task P. It is of great pleasure for me to thank my advisor, Professor L. M. Jones, for very clear and patient guidance in completing this study. I would also like to thank B. Crespi, S. A. Denham, and C. K. Ng for useful discussions.

APPENDIX: THE PHOTOINO'S ENERGY DISTRIBUTION

In this appendix I will calculate the energy distribution of each $\tilde{\gamma}$ that comes off a $\tilde{g}$ in the Θ rest frame, and calculate the total number of events with a certain missing energy.

Let us start by writing the differential decay rate of the $\tilde{g}$, according to Fig. 2:

$$d\Gamma=\frac{1}{2(2\pi)^5}\frac{1}{2E_{\tilde{g}}}\int\frac{d^3P_{\tilde{\gamma}}}{2E_{\tilde{\gamma}}}I^{\alpha\beta}\left[\sum_{\text{spins}}|M|^2\right]_{\alpha\beta}, \tag{A1}$$

where

$$I^{\alpha\beta}=\int\int\frac{d^3P_q}{2E_q}\frac{d^3P_{\bar{q}}}{2E_{\bar{q}}}P_q^{\alpha}P_{\bar{q}}^{\beta}\delta^4(P_{\tilde{g}}-P_{\tilde{\gamma}}-P_q-P_{\bar{q}})$$

and

$$\sum_{\text{spins}}|M|^2\equiv P_q^{\alpha}P_{\bar{q}}^{\beta}\left[\sum_{\text{spins}}|M|^2\right]_{\alpha\beta}$$

is the full matrix element squared for the decay. $I^{\alpha\beta}$ is a second-rank tensor[18] and can be expressed in an arbitrary Lorentz frame as

$$I^{\alpha\beta}=\frac{\pi}{24}(g^{\alpha\beta}Q^2+2Q^{\alpha}Q^{\beta})$$

with

$$Q\equiv P_{\tilde{g}}-P_{\tilde{\gamma}}\ .$$

Next we carry out the matrix-element-squared calculation together with $I^{\alpha\beta}$ in the Θ rest frame, assuming large masses for the $\tilde{q}$'s, and we find

$$\frac{d^2\Gamma}{dE_{\tilde{\gamma}}\,d\cos(\theta)}\propto|\mathbf{P}_{\tilde{\gamma}}|(-4A^2+3AB+C)\ , \tag{A2}$$

with $A\equiv P_{\tilde{g}}\cdot P_{\tilde{\gamma}}$, $B\equiv(m_{\tilde{g}}-m_{\tilde{\gamma}})^2$, and $C\equiv m_{\tilde{g}}m_{\tilde{\gamma}}(3m_{\tilde{g}}^2+3m_{\tilde{\gamma}}^2-2m_{\tilde{g}}m_{\tilde{\gamma}})$. The $\cos(\theta)$ has very complicated limits in the Θ rest frame. We can get around it by making the logical assumption that the events which contribute to the maximum value of the missing energy, all come from the forward hemisphere of the $\tilde{g}$ decay, i.e., the important events for us come for $\theta^*\leq\pi/2$ (θ^* is the angle between the $\tilde{\gamma}$'s direction and the axis of the boosting of the $\tilde{g}$, in the $\tilde{g}$'s rest frame). Boosting the $\theta^*=\pi/2$ to the Θ rest frame, we get the lower limit of the integration:

$$\cos\theta_{\min}\equiv c_m=\frac{\beta(1+Y^2)}{[(1-Y^2)^2+4\beta^2Y^2]^{1/2}}\ ,$$

where the quantities Y,β,γ are defined in Sec. IV A. Let us define the variable $x\equiv E_{\tilde{\gamma}}/m_{\tilde{g}}$; in terms of all the above variables we get, after integration over θ,

$$\left.\frac{d\Gamma}{dx}\right|^{+}\propto(x^2-Y^2)^{1/2}\{8x^2[-3\gamma^2-\gamma^2\beta^2(1+c_m+c_m^2)]+3\gamma\beta(x^2-Y^2)^{1/2}[8\gamma x-3(1-Y)^2]$$
$$\times(1+c_m)+18\gamma x(1-Y)^2+18Y-12Y^2+18Y^3+8\gamma^2\beta^2Y^2(1+c_m+c_m^2)\}\ . \tag{A3}$$

The maximum value of x is determined according to $E_{\tilde{\gamma}}^{\max}$, which was evaluated in Sec. IV A.

We can now calculate the branching ratio for the events that contribute to $E_{\max}^{\text{miss}}$, by taking the convolution of the distributions of the two $\tilde{\gamma}$'s (the two distributions are not correlated). In the convolution integral one can set

$$\gamma\simeq\frac{m_t}{m_{\tilde{g}}},\quad\frac{E_{\max}^{\text{miss}}}{2m_{\tilde{g}}}\leq x_t\leq\frac{E_{\tilde{\gamma}}^{\max}}{m_{\tilde{g}}}\ ,$$

where x_i are the energy fractions of the $\tilde{\gamma}$'s and $E_{\tilde{\gamma}}^{\max}$ is defined in Sec. IV A. The test is then to get the observed branching ratio using the calculated mass of the $\tilde{g}$.

[1]H. E. Haber and G. L. Kane, Phys. Rep. **117**, 75 (1985).
[2]W. Y. Keung, Phys. Rev. D **28**, 1129 (1983); **29**, 1544(E) (1984).
[3]R. M. Barnett, in *Supersymmmetry,* proceedings of the 13th SLAC Summer Institute on Particle Physics, Stanford, California, 1985, edited by E. C. Brenman (SLAC Report No. 296, Stanford, 1985).
[4]G. Marchesini and B. R. Webber, Nucl. Phys. **B238**, 1 (1984); B. R. Webber, *ibid.* **B238**, 492 (1984).
[5]C. K. Ng, Ph.D. thesis, University of Illinois, 1986; Phys. Rev. D **31**, 469 (1985); **33**, 3246 (1986).
[6]S. Godfrey and N. Isgur, Phys. Rev. D **32**, 189 (1985).
[7]A. De Rújula, H. Georgi, and S. L. Glashow, Phys. Rev. D **12**, 147 (1975).
[8]C. Albajar *et al.*, Phys. Lett. B **198**, 261 (1987).
[9]A. H. Mueller, Phys. Lett. **104B**, 161 (1981).
[10]The Altarelli-Parisi functions for the SUSY contents of the nucleon were calculated by several authors, e.g., S. K. Jones and C. H. Llewellyn Smith, Nucl. Phys. **B217**, 145 (1983). They were reproduced again for this study.
[11]R. Hollebeek, in *Dynamics and Spectroscopy at High Energy,* proceedings of the 11th SLAC Summer Institute on Particle Physics, Stanford, California, 1983, edited by P. M. McDonough (SLAC Report No. 267, Stanford, 1983).
[12]G. C. Fox and S. Wolfram, Nucl. Phys. **B149**, 413 (1979).
[13]W. Buchmüller, J. H. Kühn, and A. Martin, *Physics at LEP,* LEP Jamboree, Geneva, Switzerland, 1986, edited by John Ellis and Roberto Peccei (CERN Report No. 86-02, Geneva, 1986).
[14]See similar discussion on how to calculate the masses of the $\tilde{q}$ and the $\tilde{\gamma}$ for the process $e^+e^- \to Z^0 \to \tilde{q}\bar{\tilde{q}} \to q\bar{q}\tilde{\gamma}\tilde{\gamma}$, in S. A. Denham and L. M. Jones, Phys. Rev. D **34**, 3354 (1986).
[15]R. D. Peccei, in *Proceedings of the 1986 Cern School of Physics,* Sandhamn, Sweden, 1986, edited by P. O. Hulth and C. Jarlskog (CERN Report No. 87-02, Geneva, 1987).
[16]V. Barger *et al.*, Phys. Rev. D **35**, 3366 (1987); J. H. Kühn and P. M. Zerwas, Max-Planck-Institut für Physik und Astrophysik Report No. MPI-PAE/PTh 52/87 (unpublished).
[17]E. Eichten *et al.*, Phys. Rev. D **17**, 3090 (1979); **21**, 203 (1980).
[18]J. D. Bjorken and S. D. Drell, *Relativistic Quantum Mechanics* (McGraw-Hill, New York, 1964), p. 263.